Limnol. Oceanogr., 43(6), 1998, 1198–1206

Measurement of solar-stimulated fluorescence in natural waters

Chuanmin Hu[1] *and Kenneth J. Voss*
Physics Department, University of Miami, Coral Gables, Florida 33124

Abstract

The oceanic Fraunhofer line discriminator (OFLD), designed to measure the solar-stimulated inelastic scattering in the ocean, has been deployed in various types of water in Florida Bay and the Dry Tortugas to measure Fraunhofer lines and oxygen-absorption lines near 689 nm in the solar spectrum. The line-filling principle and previous work enable us to partition the measured light into elastic, Raman scattering, and fluorescence components. We show that in optically deep, oligotrophic water, where chlorophyll *a* (Chl *a*) concentration is as low as 0.1 mg m^{-3}, fluorescence near 689 nm was still measurable by the OFLD. In moderately eutrophic shallow waters, where Chl *a* concentration ranges from 0.2 to 0.8 mg m^{-3}, the fluorescence from either Chl *a* or dissolved organic matter in the water column was found to be a negligible component of the total light field due to the additional light reflected from the bottom. We also include measurements of the solar-stimulated fluorescence for benthic surfaces, such as brain coral, and have found these to be saturated under normal solar illumination.

Solar-stimulated fluorescence (or natural fluorescence) of chlorophyll *a* (Chl *a*) in the ocean is important in both remote sensing (Morel and Prieur 1977) and estimation of the photosynthetic rate (Kiefer et al. 1989), and recently has been extensively studied (Booth and Morrow 1990; Chamberlin and Marra 1992; Kiefer et al. 1989; Lizotte and Priscu 1994). As a passive technique, the measurement of natural fluorescence has advantages over active methods (laser or flashlamp as the excitation) in the sense that natural levels and spectral distributions of the excitation light are used. The in situ measurement, however, is difficult mainly because the measured light at the chlorophyll fluorescence emission band (~25 nm centered at 685 nm; Gordon 1979) is usually a sum of several components: direct or elastically scattered light, Raman scattered light by water molecules, and chlorophyll fluorescence. Thus, unless the first two are assumed to be negligible (Kiefer et al. 1989), or the measured light can be partitioned (Hu and Voss 1997), natural fluorescence cannot be obtained. Although the PNF-300 profiling natural fluorometer (Kiefer et al. 1989) is capable of measuring natural fluorescence below 6 m by assuming that the upwelling radiance, L_u(683 nm), is mainly from chlorophyll fluorescence, surface measurement is impossible since L_u(683 nm) is overwhelmed by the solar path radiance. However, our oceanic Fraunhofer line discriminator (OFLD) system has been proven effective in reducing the measured light into fluorescence and other components even at the surface (Hu and Voss 1997), thus providing us another way to measure the natural fluorescence accurately.

[1] Present address: Department of Marine Science, University of South Florida, 140 7th Ave. South, St. Petersburg, Florida 33701.

Acknowledgments

We thank A. Chapin, H. R. Gordon, and M. Monte for their help in the field measurements and model simulations, and R. G. Zika, C. A. Moore, C. Farmer, K. L. Carder, R. G. Steward, and the crew of the RV *Calanus* and *Suncoaster* for the assistance and the environmental data provided.

This work is supported by the Ocean Optics program of ONR under grants N00014-95-10309 and N00014-89-J-1985.

Methods

Light partitioning principle—The OFLD has been described elsewhere (Hu and Voss 1997; Ge et al. 1995). It is mainly composed of two fiberoptic light collectors, an OMA CCD camera, and a high-resolution SPEX 1000M monochromator. The whole system has a resolution of ~0.008 nm per CCD pixel, enough to resolve the ~0.1 nm Fraunhofer absorption peak. The working principle of the OFLD is simple: because the inelastically scattered light at depth will add equally to both the absorption line peak and the spectrum background continuum, the addition of inelastic light will cause the apparent absorption line size to decrease. A measure of the line size at depth, z, is given by the equivalent width, $w(z)$, defined by

$$w(z) = \int_{\lambda_1}^{\lambda_2} \left[1 - \frac{E(\lambda, z)}{E_b(\lambda, z)}\right] d\lambda. \quad (1)$$

Here, λ_1 and λ_2 are the starting and ending points of the Fraunhofer line, $E(\lambda, z)$ is the spectral irradiance, and $E_b(\lambda, z)$ is the background irradiance, which is defined as a straight line between $E(\lambda_1, z)$ and $E(\lambda_2, z)$. w_0 is simply the $w(0)$, the equivalent width of the absorption line in the downwelling light spectrum at the sea surface. Thus, by measuring a solar Fraunhofer line and comparing $w(z)$ with w_0, the inelastic contribution in the measured light at depth z is obtained by (Hu 1997)

$$\frac{E_{in}(z)}{E_t(z)} = 1 - \frac{w(z)}{w_0}, \quad (2)$$

where the total measured light, $E_t(z)$, is a sum of three sources: $E_{el}(z)$ from direct solar transmission and elastic scattering, $E_r(z)$ from Raman scattering, and $E_f(z)$ from fluorescence

$$E_t(z) = E_{el}(z) + E_r(z) + E_f(z), \quad (3)$$

and $E_{in}(z)$ is just a sum of the two inelastic scattering terms

$$E_{in}(z) = E_r(z) + E_f(z). \quad (4)$$

Table 1. Environmental data for some of the measurement stations in Florida Bay and the Dry Tortugas. C was obtained from Zika et al. (pers. comm.) and Carder and Steward (pers. comm.) (n.a., not available).

Sta.	Date	GPS	Bottom (m)	θ_0	Wind (m s^{-1})	C (mg m^{-3})	DOM (QSU)
1	1 May 96	25.02.05N, 80.08.07W	None	~15°	~5	~0.1	n.a.
2	13 Jul 96	24.38.03N, 82.56.48W	~17	~5°	~3.5	~0.4	n.a.
3	27 Apr 96	25.19.45N, 81.07.06W	~3.5	~22°	~1.2	~0.8	34.0
4	12 Jul 96	24.37.42N, 82.56.48W	~7.9	2° to ~35°	~2	~0.4	n.a.

In practice, the measured light E_t can be either downwelling irradiance E_d, upwelling irradiance E_u, or the upwelling nadir radiance L_u. From previous work (Hu and Voss 1997), $E_r(z)$ has been measured and modeled in the downwelling and upwelling irradiance fields, and therefore $E_f(z)$ can be separated out from the measured $E_t(z)$.

Oxygen absorption lines—In order to study the chlorophyll fluorescence at 685 nm, we need to use a Fraunhofer line in that region. Unfortunately, the Fraunhofer lines in this region are too small; therefore, we use the atmospheric oxygen absorption lines around 689 nm as an alternative (Carter et al. 1996). Unlike the Fraunhofer lines, which are caused by the solar constituents, these absorption lines are proportional to the atmospheric pathlength and thus to time (or solar zenith angle θ_0). Thus, we restricted this technique to periods around solar noon, when the pathlength ($1/\cos\theta_0$) was approximately constant, to reduce the error caused by the variation in w_0. However, with simultaneous measurement of w_0 the technique can be extended to other times.

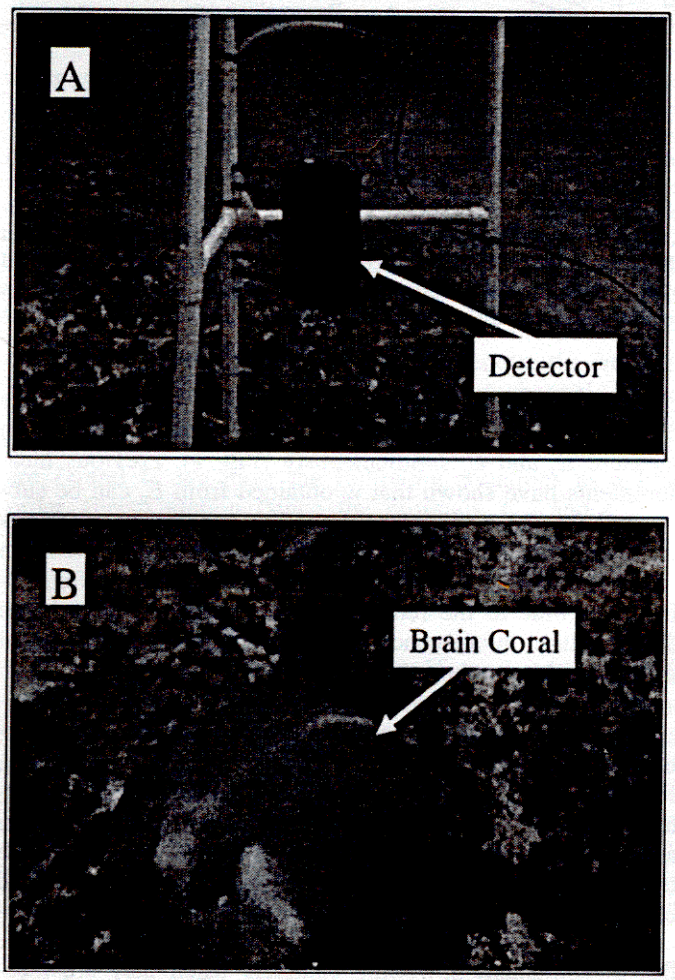

Fig. 1. Configuration of measurement on benthic surfaces. The OFLD detector is hooked to a tripod frame (A) and a radiance collector is used to look at a spot, such as a brain coral (B).

Field measurements—The instrument was deployed in Florida Bay and the Dry Tortugas. The water type ranged from deep clear water to shallow coastal water rich in pigments and dissolved organic matter. The environmental data for some of the measurement stations are listed in Table 1. Pigment data were collected by other groups (R. G. Zika et al. pers. comm.; Carder and Steward pers. comm.). When the upwelling irradiance, E_u, or the nadir upwelling radiance, L_u, just beneath the surface were measured, the detector head was suspended from a float (Hu 1997) that was separated from the ship to minimize the ship shadowing effect. The radiance collector is in fact a bare fiber protected by transparent glass and it has a full view angle of ~20° in water. It can be used to study a localized spot or sample, such as

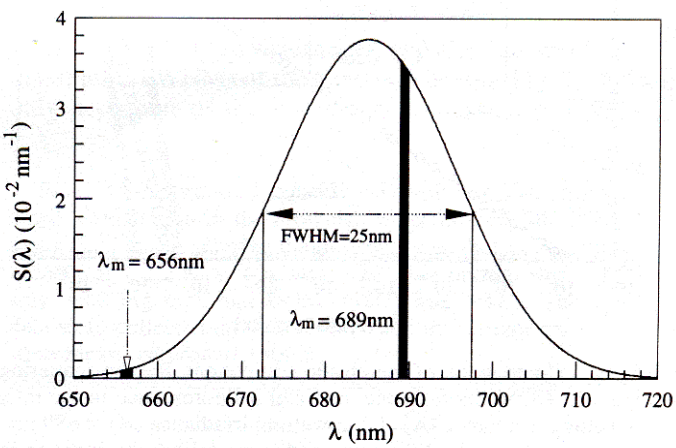

Fig. 2. Simulated Chl *a* fluorescence. Photons emitted in the 689-nm narrow band occupy only 3.5% of the whole emission band. For the 656-nm narrow band, the percentage is only 0.1%.

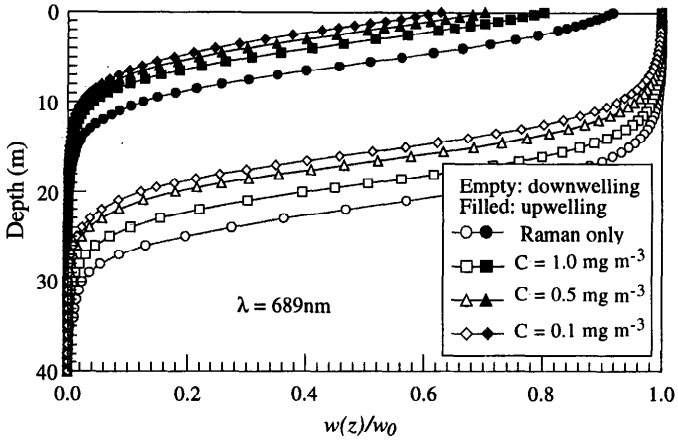

Fig. 3. Effect of Chl *a* fluorescence on the light field at 689 nm. In the model, θ_0 is 15°, wind speed is 5 m s^{-1}, DOM absorption at 380 nm is 0.05 m^{-1}, a_c*(440) is 0.034 m^2 mg^{-1}, and the fluorescence quantum yield is 0.7%. *C* is the Chl *a* concentration and is assigned several values in the model.

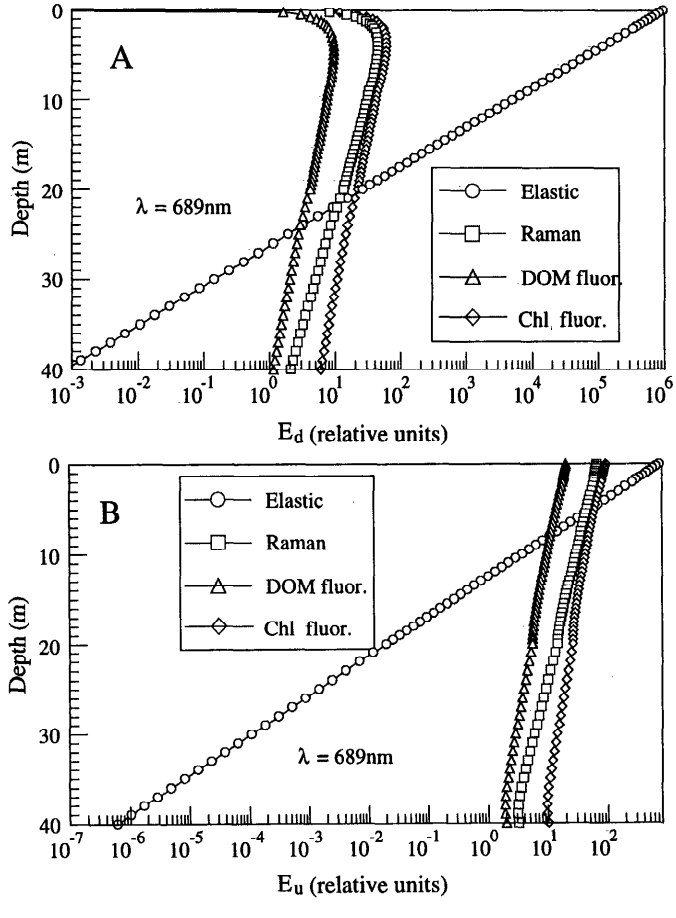

Fig. 4. Comparison of the elastic component, Raman scattering component, DOM fluorescence, and Chl *a* fluorescence in the total downwelling irradiance (A) and upwelling irradiance (B) at 689 nm. *C* is 0.1 mg m^{-3}, and other inputs of the model are the same as in Fig. 3. Although DOM fluorescence is negligible in both E_d and E_u at low concentrations, Chl *a* fluorescence is comparable or even larger than Raman scattering.

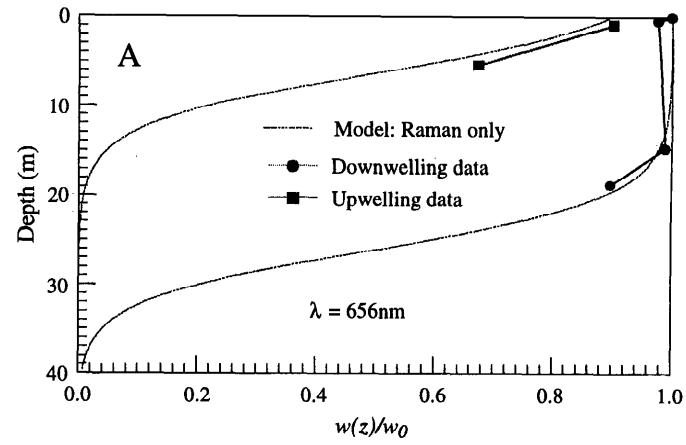

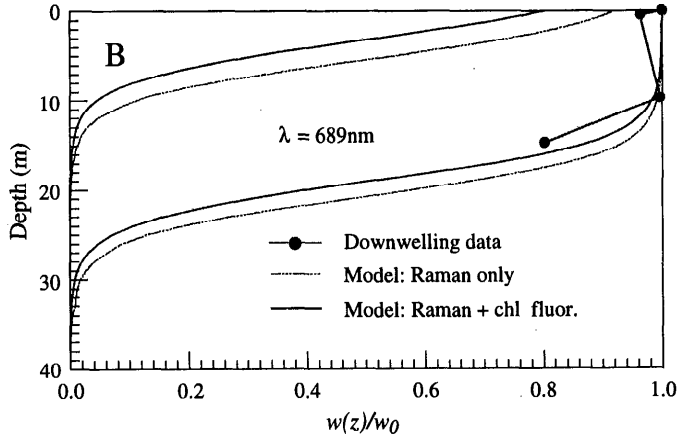

Fig. 5. Results from Sta. 1 at 656 nm (A) and 689 nm (B). In the model, θ_0 is 15°, wind speed is 5 m s^{-1}, *C* is 0.1 mg m^{-3}, and η is 0.7%. In panel B, fluorescence is detected at 689 nm in addition to Raman scattering.

coral in the Dry Tortugas (Fig. 1). In the Dry Tortugas where the water is shallow, the detector was put on the bottom to measure E_d and L_u simultaneously (Fig. 1). Previous measurements have shown that *w* obtained from E_d can be substituted for the surface w_0 in shallow water (Hu 1997), as water-column inelastic sources are insignificant. In addition to the measurement at 689 nm, several other Fraunhofer lines from the blue to the red range were measured in order to detect natural fluorescence caused by sources other than Chl *a* (e.g. DOM or other pigments).

Data reduction—The goal of the instrument data reduction is to obtain the normalized equivalent width, $w(z)/w_0$, from the raw data on the CCD, which are in units of electronic counts vs. CCD pixels. As described previously (Hu and Voss 1997), several procedures are applied to remove the dark current, perform the wavelength calibration, and remove additional sources of noise. In addition, a new procedure is required to remove the crosstalk between the downwelling and upwelling channels when they are measured simultaneously (e.g. for the data collected in the Dry Tortugas). In this procedure, the downwelling and upwelling channels are measured separately at the surface, and the

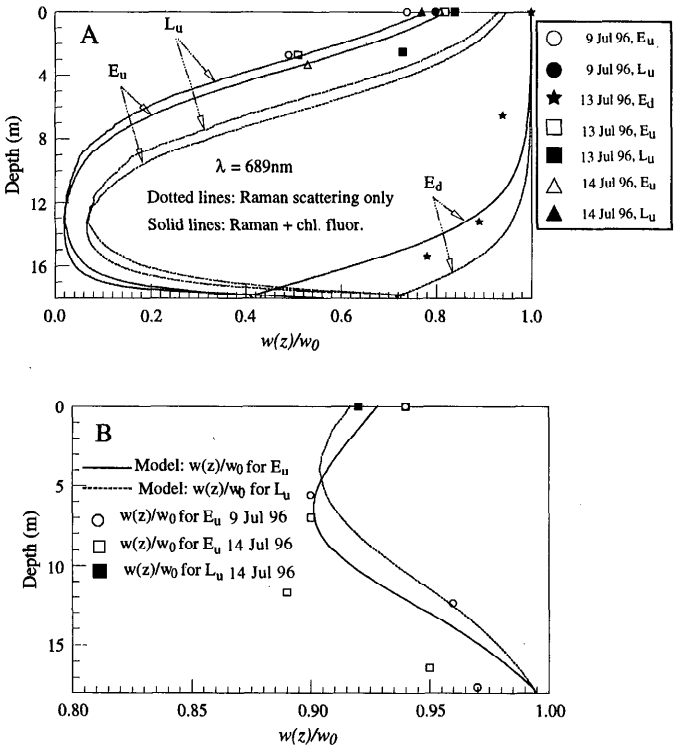

Fig. 6. Comparison between model simulations and measurements at 689 nm (A) and 589 nm (B) from Sta. 2. In the model, θ_0 is 5°, wind speed is 2 m s^{-1}, C is 0.5 mg m^{-3} (Carder and Steward pers. comm.), and η is 0.3%. In panel A, fluorescence can be derived by subtracting the Raman scattering contribution from the measured inelastic percentage in the upwelling light. The increases of $w(z)/w_0$ when approaching the bottom are caused by the bottom effect, which was detected by the OFLD at the same spot at 589 nm (B).

crosstalk C_{du} and C_{ud} are computed (*du* denotes the crosstalk from downwelling channel onto upwelling channel, and *ud* for crosstalk from upwelling to downwelling channel). If the simultaneous measured downwelling and upwelling spectra are D and U, we have the following equations as a first-order approximation (since the crosstalk C_{du} and C_{ud} are small, <1% of the total measured signal):

$$D' + C_{ud}U' = D, \tag{5}$$

and

$$C_{du}D' + U' = U, \tag{6}$$

and thus the true downwelling and upwelling spectra D' and U' can be derived accordingly. Because the upwelling signal is usually much smaller than the downwelling one, in practice only the crosstalk from the downwelling channel is removed and we have $D' \approx D$ and $U' \approx U - C_{du}D$, respectively. In laboratory experiments we have found that this procedure can correct the w from the upwelling channel to its true value within 2% error. Our estimated total error in reducing the $w(z)$ data is estimated to be <10%.

Model simulations—From Eq. 2–4, the total inelastic light, E_{in}, in the measured light at depth, E_t, can be determined as

Table 2. Normalized equivalent width, $w(z)/w_0$, from the 26 April 1996 station in the coastal greenish water of Florida Bay. During the measurement, there were scattered clouds, wind speed was ~3 m s^{-1}, θ_0 was ~30°, sea bottom was ~3.5 m, C was ~0.8 mg m^{-3}, and DOM (QSU) was ~5.9. L_u in the table is the nadir upwelling radiance.

	λ_f (nm)					
z (m)	689	656	589	518	486	434
1.5 (E_d)	0.99	0.98	0.96	0.98	0.99	1.02
3.1 (E_u)	0.95	0.99	0.97	0.99	1.05	1.03
0.9 (L_u)	0.98	0.97	0.99	0.96	1.05	1.04

$$E_{in} = E_r + E_f = \left[1 - \frac{w(z)}{w_0}\right]E_t, \tag{7}$$

where E_r is due to Raman scattering and E_f is a sum of both DOM and Chl *a* fluorescence. Raman scattering can be modeled (Ge et al. 1993; Hu and Voss 1997), therefore, by putting the environmental factors of the data collection station, such as the pigment concentration, the wind speed (related to sea surface roughness), and the solar zenith angle, into the model, and the Raman scattering component can be separated from E_{in}, thus leaving the fluorescence.

By knowing the concentration of the fluorescent material, fluorescence can also be modeled and compared with measurement to determine the fluorescence efficiency. The influence of DOM fluorescence on the $w(z)/w_0$ profile has been modeled by Ge et al. (1995)—fluoresced photons are generated according to the fluorescence efficiency (Hawes et al. 1992) and the depth-dependent excitation source, which is computed by a Monte Carlo model. These photons propagate according to the attenuation properties at the emission wavelength, and the fluorescence contribution to the light field at the emission wavelength is obtained.

Chl *a* fluorescence is centered at 685 nm and has an approximately Gaussian-shape emission band with the shape factor given by Gordon (1979)

$$S(\lambda_m) = \frac{1}{(2\pi\sigma^2)^{1/2}}\exp\left(-\frac{(\lambda_m - 685)^2}{2\sigma^2}\right), \tag{8}$$

where $\sigma \approx 10.6$ nm determines that the full width at half-maximum (FWHM) of the band is ~25 nm (Fig. 2). Because only a portion of the fluorescence emission contributes to

Table 3. Normalized equivalent width, $w(z)/w_0$, from the 27 April 1996 station in the brownish water in the Little Shark River along Florida Bay. During the measurement, the sky was clear, wind speed was ~1.2 m s^{-1}, θ_0 was ~22°, sea bottom was ~3.5 m, C was ~0.8 mg m^{-3}, and DOM (QSU) was ~34.0. The upwelling data were collected around 1100 h, and the surface reference lines were measured around 1500 h.

	λ_f (nm)				
z (m)	689	656	589	518	486
0.8 (E_u)	1.06	1.02	1.02	1.06	1.03
3.0 (E_u)	1.06	1.03	1.05	1.04	0.99

Table 4. Normalized equivalent width, $w(z)/w_0$, from the 29 April 1996 station in the coastal greenish water of Florida Bay. During the measurement, the sky was clear with scattered clouds, wind speed was ~10 m s^{-1}, θ_0 was ~40°, and the sea bottom was ~5 m. The detector unit was hooked to a surface float to measure the surface upwelling signal.

	λ_f (nm)					
z (m)	689	656	589	518	486	434
0.2 (E_u)	0.99	0.98	0.97	0.96	1.00	1.05
0.2 (L_u)	1.00	1.00	0.97	0.98	1.04	1.03

the 689-nm oxygen absorption line (688.75–689.82 nm) and the 656-nm Fraunhofer line (655.63–657.04 nm), in terms of the fluorescent efficiency at the emission band per unit wavelength, a parameter, η_{λ_m}, is defined as

$$\eta_{\lambda_m} = \frac{\int_{\lambda_1}^{\lambda_2} S(\lambda)\, d\lambda}{\int_{400}^{700} S(\lambda)\, d\lambda} \frac{1}{\lambda_2 - \lambda_1} \eta(\lambda_e)\ (\text{nm}^{-1}), \quad (9)$$

where $\eta(\lambda_e)$ is the normally used quantum yield (photons fluoresced over photons absorbed), λ_1 and λ_2 are 688.75 and 689.82 nm for λ_m of 689 nm and 655.63 and 657.04 nm for λ_m of 656.28 nm, respectively (Fig. 2). Therefore, we have $\eta(689)$ of $0.035\eta(\lambda_e)$ (nm^{-1}) and $\eta(656)$ of $0.001\eta(\lambda_e)$ (nm^{-1}).

Similar to the DOM fluorescence model (Ge et al. 1995), the contribution of Chl *a* fluorescence to the downwelling irradiance at the emission wavelength, λ_m, is expressed as

$$E_d^{Chl}(z, \lambda_m) \cong \frac{1}{2} \int_0^z \left[\int_{\lambda_e} \frac{\lambda_e}{\lambda_m} \eta_{\lambda_m} a_c(\lambda_e) D_d E_d(0, \lambda_e) \times \prod_{z_i=0}^{z'} \exp(-K_d(\lambda_e, z_i)\Delta z_i)\, d\lambda_e \right] \times \prod_{z_i=z'}^{z} \exp(-K_u(z_i, \lambda_m)\Delta z_i)\, dz', \quad (10)$$

where the E and the K values are obtained from the Monte Carlo model, D_d is the distribution function and is taken to be 1.18 as in the DOM fluorescence model, $a_c(\lambda_e)$ is the absorption coefficient of phytoplankton in units of m^{-1}. The upwelling term of fluorescence is computed similarly by replacing the integral limits, 0 to z, in Eq. 10 with ∞ to z.

One important parameter in Eq. 10 is the spectral absorption coefficient of phytoplankton, $a_c(\lambda_e)$, which is a product of Chl *a* concentration, C, and the Chl *a*-specific absorption, $a_c^*(\lambda_e)$, in units of m^2 mg^{-1}. $a_c^*(\lambda_e)$ has been measured many times (Bricaud et al. 1995 and references therein). Although the overall shape of the spectral response remains the same, there are two strong absorption bands around 440 nm and 670 nm; differences exist because of the complexity in the auxiliary pigments in the phytoplankton family. The absolute value of $a_c^*(440)$ also varies due to many factors, such as the pigment-packaging effect (Kirk 1975; Morel and Bricaud 1981), which is dependent on the ambient irradiance field. Gordon's (1992) value, $a_c^*(440) = 0.034$ m^2 mg^{-1}, explains Morel's (1988) statistical data very well and is used in this model. The spectral response of $a_c^*(\lambda_e)$ is taken from Morel (1988).

Another key parameter in the model is the fluorescence quantum yield, $\eta(\lambda_e)$. $\eta(\lambda_e)$ is generally thought to be independent of λ_e (Forster and Livingston 1952; Gordon 1992); that is, it is a constant over the excitation band. It is a variable of many environmental factors, such as the growth environment and the composition of the phytoplankton species. Values of $\eta(\lambda_e)$ have ranged from <1% to 10% (Mobley 1994). We used the value of 0.7% to account for absorption by other particulates included in our model (Gordon 1979).

A sample simulation result is given in Fig. 3 to illustrate the effect of Chl *a* fluorescence on the $w(z)/w_0$ profile at 689 nm. In the model, the solar zenith angle θ_0 is 15°, wind speed is 5 m s^{-1}, DOM absorption at 380 nm, $a_y(380)$, is 0.05 m^{-1} and Chl *a* concentration, C, is assumed to be constant for the whole water column and it varies from 0.1 to 1.0 mg m^{-3}. The fluorescence quantum yield is 0.7%. It is clearly shown that Chl *a* fluorescence can alter the profile considerably, even at a low pigment concentration. For the same environmental inputs and C of 0.1 mg m^{-3}, Fig. 4 shows a comparison of all components in the total irradiance light field at 689 nm. Although DOM fluorescence is small, Chl *a* fluorescence is comparable to or even larger than Raman scattering for both E_d and E_u. For upwelling light (Fig. 4B), E_u^{Chl} is much larger than E_u^{el} below 6 m, which confirms the assumption of Kiefer et al. (1989). However, E_u^{Raman} cannot be neglected even in deep water when Chl *a* concentration is small.

At 656 nm, Chl *a* fluorescence contributes a negligible amount of light to both E_d and E_u. This is because 656 nm is almost outside the fluorescence emission band (Fig. 2).

Results and discussion

Deep clear water—At Sta. 1 (Table 1), the water was deep and clear, and pigment data collected at a nearby station indicated that C was ~0.1 mg m^{-3}. Simulation results indicate that although Raman scattering is the primary source of inelastic light at 656 nm (Fig. 5A), Chl *a* fluorescence must be considered together with Raman scattering in order to explain the inelastic contribution to the downwelling light field at 689 nm (Fig. 5B). At 15 m, the model shows that the contributions of Raman scattering and Chl *a* fluorescence to the downwelling irradiance are ~7% and ~13%, respectively.

At Sta. 2 and two other similar shallow (18 m) water stations in the Dry Tortugas, L_u was measured in addition to E_u. The reduced data are shown in Fig. 6 together with the model simulations. At those stations the bottom is mainly composed of sand and calcareous sediments, with scattered coral and sea plants. For the sake of simplicity, the bottom is assumed to be a lambertion reflector with a reflectance of 0.2 in the model. The fluorescence quantum yield η was tuned to be 0.3%, which is much smaller than the value used by Gordon (1979). This could reflect a variation in a_c^* or

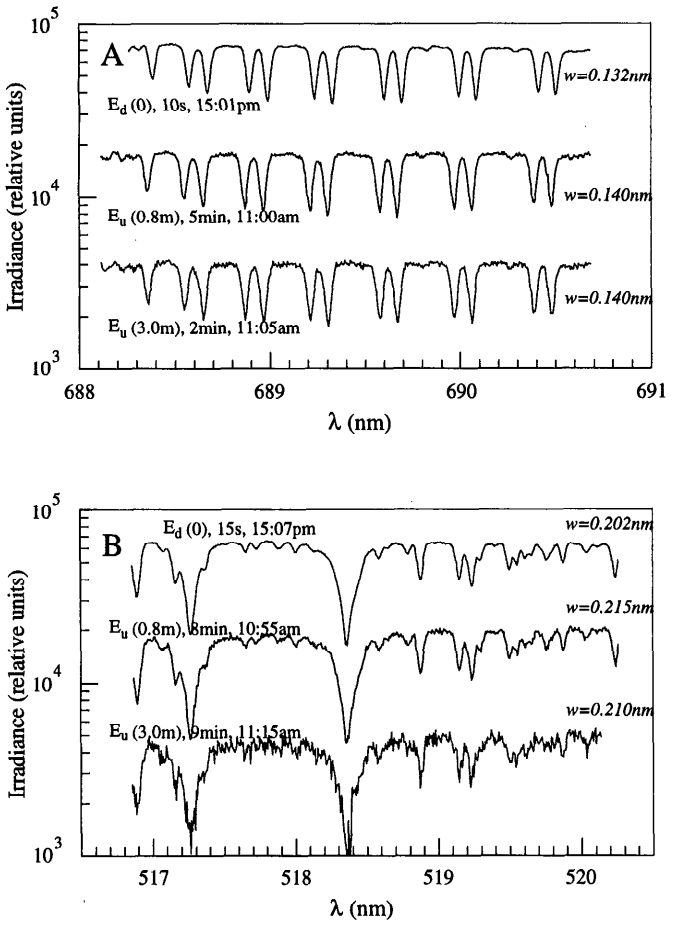

Fig. 7. At Sta. 3 (Shark River), where the water is brownish and rich in pigments and DOM, spectra measured by the OFLD at 689 nm (A) and 518 nm (B). No line filling was detected in the upwelling light due to the 3.5-m water depth.

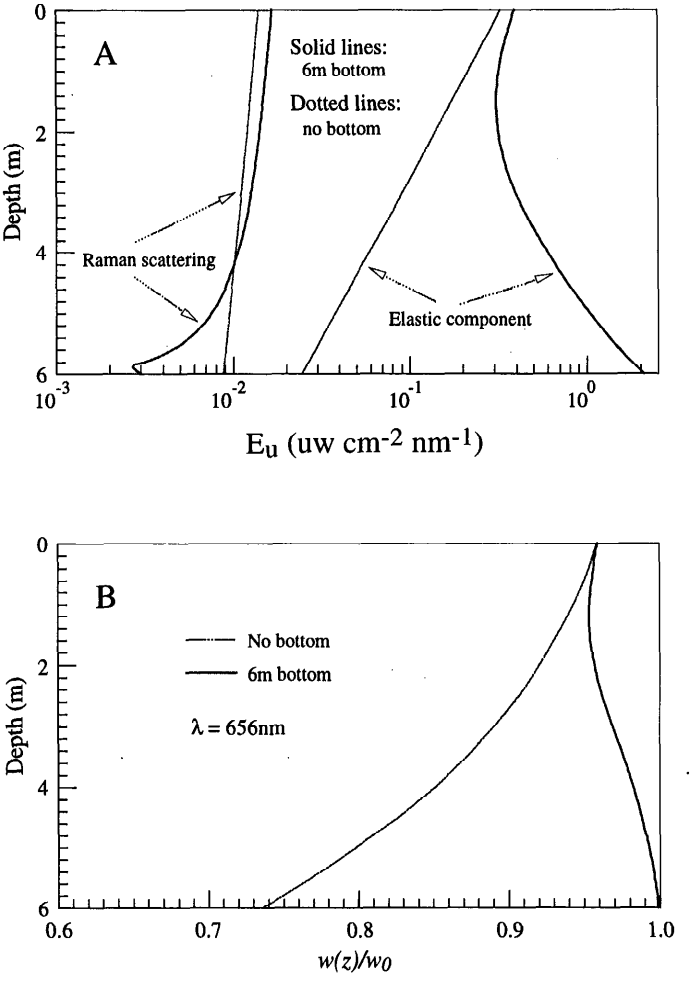

Fig. 8. The bottom effect on the upwelling irradiance light field. In the model, θ_0 is 20°, wind speed is 5 m s^{-1}, C is 1 mg m^{-3}, and the bottom reflectance is 0.2. The elastic component in E_u with a water depth of 6 m is much larger than for the optically deep situation (A) owing to the bottom reflection. The Raman scattering contribution varies slightly, and therefore $w(z)/w_0$ approaches 1.0 above the bottom (B). In panel A, E_u is normalized to the extraterrestrial solar irradiance spectrum.

the fluorescence efficiency due to the highlight environment. Fig. 6A shows clearly that Chl *a* fluorescence was detected in the upwelling light. From the surface to 4 m in water, a comparison between the data and the Raman scattering model shows that the fluorescence percentage in E_u and L_u increases from 15 to 42%, while the Raman scattering contribution ranges from 5 to 17%. Note that when approaching the bottom, the model shows that the elastic part dominates the upwelling light field again, i.e. there is a turning point in the $w(z)/w_0$ profile. This is due to the bottom effect, as will be shown later. This effect was measured at the same station at 589 nm where the light transmission is much higher than at 689 nm. Fig. 6B shows the agreement between the measurement and the model. Because the bottom reflection properties are unknown, the 0.2 reflectance assumption was only able to qualitatively explain the behavior near the bottom.

Shallow coastal water—Generally, the shallow water in Florida Bay is rich in pigments and DOM. For the stations measured, C ranged from 0.2 to 0.8 mg m^{-3} and DOM level varied from 1 to 34 (QSU) (~0.4 for the clear water in the Florida Straits) (Zika et al. pers. comm.). Data reduced from several stations are presented in Tables 2 to 4. In no region of the spectrum does the inelastic light make a significant contribution. As an example, the spectra at 689 and 518 nm from the brownish Shark River water are presented in Fig. 7. Even in this high-pigment, high-DOM water there is no measurable line filling. This is due to the light reflected from the bottom. This reflected light increases the upwelling light considerably, while the inelastic part remains virtually unchanged; therefore, the upwelling light contains a negligible inelastic component. Figure 8 illustrates the results of a model calculation for shallow water including a bottom effect. In fact, even if the bottom reflectance is zero, the inelastic percentage in the upwelling light decreases. Although the elastic part is smaller than in deep water, the inelastic part drops faster (Hu 1997). Consequently, in these shallow waters, Raman scattering or fluorescence is not detected. Mea-

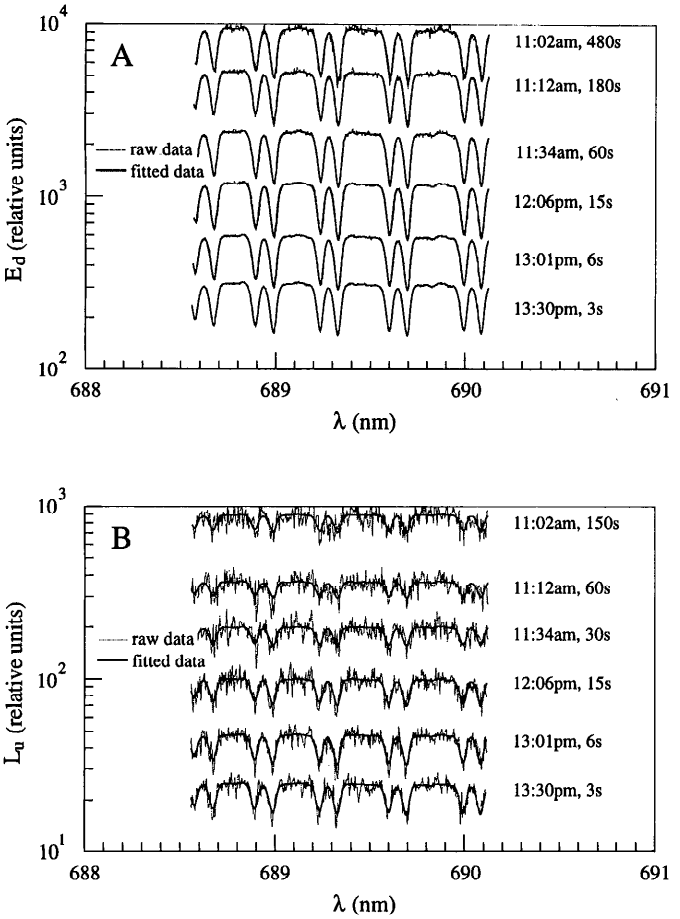

Fig. 9. Downwelling irradiance spectra (A) and upwelling radiance spectra (B) at 689 nm simultaneously measured on a brain coral (Fig. 1) in the Dry Tortugas. The top three spectra in both panels were obtained when the radiance collector was 0.2 m from the coral surface, while the others were obtained when the distance was 1.0 m. The fitting procedure (Hu and Voss 1997) was used to obtain the clean spectra from the noisy data in panel B.

surements of the shallow waters in the Dry Tortugas give the same result. Thus, once inelastic light is detected in a similar water body, it must be attributed to fluorescence of the bottom. This enabled us to measure the fluorescence from various benthic surfaces in the Dry Tortugas as part of the Coastal Benthic Optical Properties (CoBOP) program sponsored by the Office of Naval Research (ONR).

Coral reef—On 12 July 1996, the detector head was placed viewing a brain coral to simultaneously measure E_d and L_u at several wavelengths. Figure 9 shows $E_d(689)$ and $L_u(689)$ spectra from the morning to solar noon. The line filling is clearly seen by comparing Fig. 9A and Fig. 9B. Previous work and the model simulations have shown that for E_d at this depth (~7.3 m from the surface), $w(z)$ is equal to w_0, and therefore we can use Fig. 9A as a reference to normalize the data in Fig. 9B. The result, together with the 656-nm data, is presented in Fig. 10. From Eq. 2–4, because Raman scattering contributes virtually nothing to the upwelling light, we have

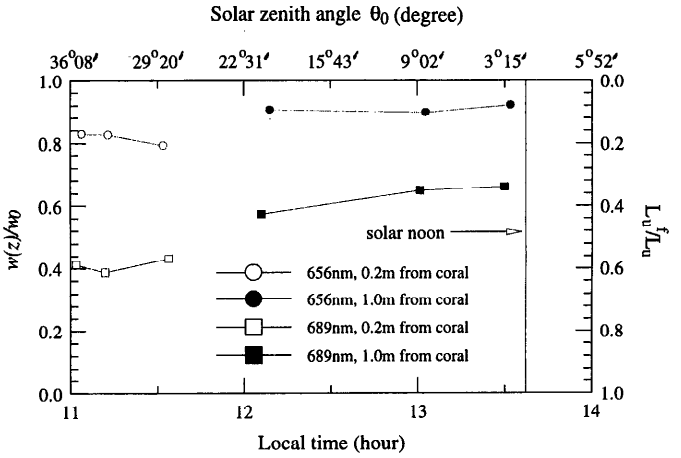

Fig. 10. The absorption line size, $w(z)$, for the $L_u(689)$ spectra (Fig. 9B), normalized to the line size (w_0) for the corresponding $E_d(689)$ spectra (Fig. 9A), as a function of local time and the corresponding solar zenith angle. Also shown in the figure is the result from the 656-nm Fraunhofer line measurement. The fluorescence component, L_u^f, in L_u is obtained accordingly.

$$L_u^f = \left[1 - \frac{w(z)}{w}\right] L_u \tag{11}$$

and

$$L_u^{el} = \frac{w(z)}{w} L_u, \tag{12}$$

where L_u^f and L_u^{el} are the fluorescence and elastic components in the total measured L_u. Note that the distance between the radiance collector and the coral surface was changed during the measurement, from 0.2 to 1.0 m. How-

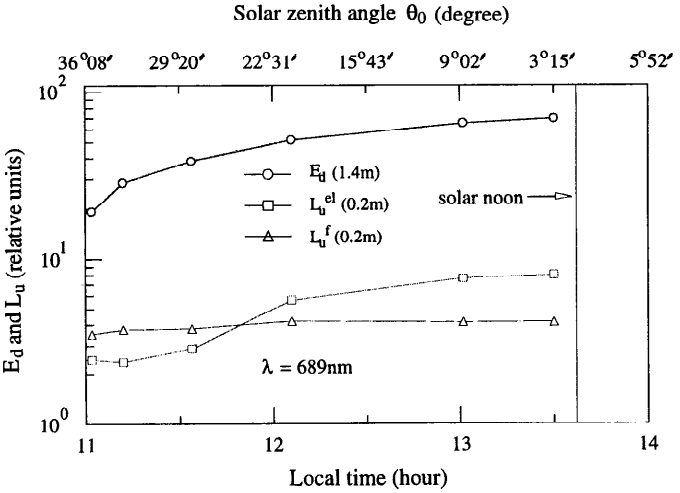

Fig. 11. Partition of $L_u(689)$ from Fig. 9B according to Eq. 11 and 12. The two distances used in the measurement were converted to one distance by Eq. 13 for comparison. The distance in the brackets refers to the coral surface. This shows that while the elastic component in $L_u(689)$, L_u^{el}, increases with the incident light, $E_d(689)$, the fluorescence component, L_u^f, remains virtually unchanged.

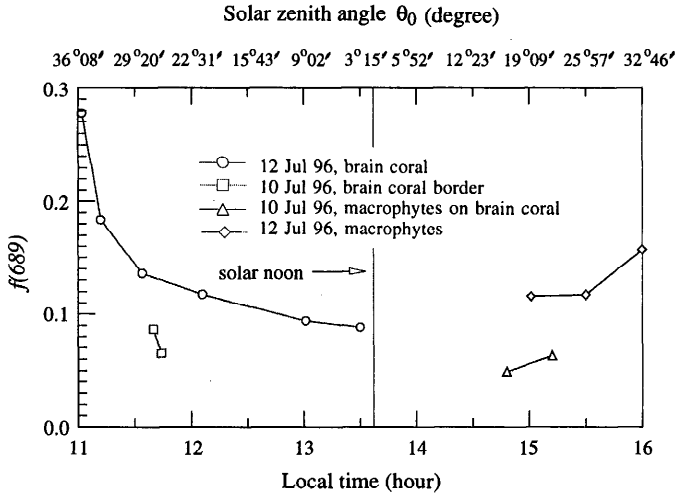

Fig. 12. Inelastic reflectance at 689 nm, $f(689)$, which is the ratio of $L_u^f(689)$ over $E_d(689)$ in Fig. 11 but with the values converted to the coral surface, drops from the morning to solar noon. Measurements from other surfaces also show the tendency of $f(689)$ to reach the minimum around solar noon.

ever, assuming that the coral surface is homogeneous over the measurement scale (the viewing area on the coral is ~0.13 m^2 when the radiance collector is 1.0 m from it), by using the radiance invariance law we can convert $L_u(1\text{ m})$ to $L_u(0.2\text{ m})$ by

$$L_u(0.2\text{ m}) = L_u(1\text{ m}) \times \exp[K_w(1 - 0.2)], \quad (13)$$

where K_w is the diffuse attenuation coefficient of seawater and is ~0.5 m^{-1} at 689 nm for the station. E_d can be converted similarly. The results are presented in Fig. 11. As can be seen from the figure, although $E_d(689)$ increases from the morning to solar noon, as does $L_u^{el}(689)$, the fluorescence contribution to the upwelling radiance, $L_u^f(689)$, seems to be saturated over the measurement period.

A parameter, inelastic reflectance f, defined as $G\pi L_u^f/E_d$, where G is a calibration constant, can be used to describe the fluorescent properties of the surface. Here, L_u^f and E_d are at the coral surface and they can be converted from the values shown in Fig. 11. Let G equal $1/\pi$; $f(689\text{ nm})$ as a function of time is drawn in Fig. 12. It is shown that $f(689)$ drops from the morning to solar noon. Measurements on other benthic surfaces, such as macrophytes, also show that $f(689)$ tends to reach its minimum around solar noon (Fig. 12). This is in agreement with many published results for phytoplankton (Kiefer 1973; Gerber and Hader 1995; Bilger et al. 1995), and may be attributed to nonphotochemical quenching and photoinhibition. Nonphotochemical quenching usually occurs at high input light levels, and the threshold for the phytoplankton communities may vary from 1.5 × 10^{15} quanta cm^{-2} s^{-1} in deep water to 2.5 × 10^{16} quanta cm^{-2} s^{-1} in surface water (Falkowski et al. 1994). The threshold that causes photoinhibition is even higher. On the other hand, a typical value for the solar irradiance in visible spectrum is ~5 × 10^{16} quanta cm^{-2} s^{-1} at a depth of 8 m in clear water when the sky is clear and θ_0 is ~5°. This is far beyond the threshold values. Therefore, nonphotochemical quenching and photoinhibition may cause the variation of $f(689)$ with time. The low value of quantum efficiency (0.3%) in Fig. 6 might be caused by these processes as well. Note that this phenomenon should occur for all the fluorescent bottoms in shallow water. Another explanation could arise from a purely optical standpoint. As θ_0 increases, the spectral distribution of light will shift to the wavelength of minimum attenuation (blue to blue-green). Therefore, $E_d(689)$ would decrease faster with increasing θ_0 than irradiance in the blue wavelength. Because fluorescence shifts light from blue to red, there would be more fluorescence per $E_d(689)$ with larger θ_0, and $f(689)$ would increase. In any case, further investigation is needed to determine the exact cause for the variation of $f(689)$.

Conclusions—Through a series of field measurements, it has been shown that as a passive method, the OFLD is capable of measuring the solar-stimulated in situ fluorescence. The chlorophyll fluorescence portion in the upwelling light at 689 nm is found to increase from 15% at the surface to 42% at 4 m in the 18-m water around the Dry Tortugas. In shallow waters (depth of <6 m) in Florida Bay, Raman scattering and fluorescence were found to be a negligible portion of the total light field due to the bottom effect.

This new technique enables us to measure the natural fluorescence of Chl *a* even in the presence of a significant amount of direct solar light, such as in the surface water, or for fluorescent benthic surface. In addition, natural fluorescence by DOM can also be estimated when light at other Fraunhofer wavelengths (e.g. 486, 518, 589 nm) is measured by the OFLD. However, because the OFLD is not absolutely calibrated, and the PAR is not measured, estimates of the fluorescence quantum yield are not possible from this measurement.

References

BILGER, W., U. SCHREIBER, AND M. BOCK. 1995. Determination of the quantum efficiency of photosystem II and of non-photochemical quenching of chlorophyll fluorescence in the field. Oecologia **102:** 425–432.

BOOTH, C. R., AND J. H. MORROW. 1990. Measuring ocean productivity via natural fluorescence. Sea Technol. **31:** 33–38.

BRICAUD, A., M. BABIN, A. MOREL, AND H. CLAUSTRE. 1995. Variability in the chlorophyll-specific absorption coefficients of natural phytoplankton: Analysis and parameterization. J. Geophys. Res. **100:** 13,321–13,332.

CARTER, G. A., J. H. JONES, R. J. MITCHELL, AND C. H. BREWER. 1996. Detection of solar-excited chlorophyll *a* fluorescence and leaf photosynthetic capacity using a Fraunhofer line radiometer. Remote Sens. Environ. **55:** 89–92.

CHAMBERLIN, S., AND J. MARRA. 1992. Estimation of photosynthetic rate from measurements of natural fluorescence: Analysis of the effects of light and temperature. Deep-Sea Res. **39:** 1695–1706.

FALKOWSKI, P. G., R. GREENE, AND Z. KOLBER. 1994. Light utilization and photoinhibition of photosynthesis in marine phytoplankton, p. 407–432. *In* N. R. Baker and J. R. Bowyer [eds.], Photoinhibition of photosynthesis. BIOS Sci. Publ.

FORSTER, L. S., AND R. LIVINGSTON. 1952. The absolute quantum yields of the fluorescence of chlorophyll solutions. J. Chem. Phys. **20:** 1315–1320.

GE, Y., H. R. GORDON, AND K. J. VOSS. 1993. Simulation of inelastic-scattering contributions to the irradiance field in the ocean: variation in Fraunhofer line depths. Appl. Optics **32:** 4028–4036.

———, K. J. VOSS, AND H. R. GORDON. 1995. In situ measurements of inelastic light scattering in Monterey Bay using solar Fraunhofer lines. J. Geophys. Res. **100:** 13,227–13,236.

GERBER, S., AND D. HADER. 1995. Effects of enhanced solar irradiation on chlorophyll fluorescence and photosynthetic oxygen production of five species of phytoplankton. FEMS Microbiol. Ecol. **16:** 33–42.

GORDON, H. R. 1979. Diffuse reflectance of the ocean: The theory of its augmentation by chlorophyll *a* fluorescence at 685 nm. Appl. Optics **18:** 1161–1166.

———. 1992. Diffuse reflectance of the ocean: Influence of nonuniform phytoplankton pigment profile. Appl. Optics **31:** 2116–2129.

HAWES, S. K., K. L. CARDER, AND G. R. HARVEY. 1992. Quantum fluorescence efficiencies of fulvic and humic acids: Effects on ocean color and fluorometric detection. Ocean Optics XI, Proc. SPIE **1750:** 212–223.

HU, C. 1997. In situ measurement of inelastic light scattering in natural waters. Ph.D diss., Univ. Miami.

———, AND K. J. VOSS. 1997. In situ measurement of Raman scattering in clear ocean water. Appl. Optics **36:** 6962–6967.

KIEFER, D. A. 1973. Chlorophyll *a* fluorescence in marine centric diatoms: Responses of chloroplasts to light and nutrient stress. Mar. Biol. **23:** 39–46.

———, W. S. CHAMBERLIN, AND C. R. BOOTH. 1989. Natural fluorescence of chlorophyll *a*: Relationship to photosynthesis and chlorophyll concentration in the western South Pacific gyre. Limnol. Oceanogr. **34:** 868–881.

KIRK, J. T. O. 1975. A theoretical analysis of the contribution of algal cells to the attenuation of light within waters. II. Spherical cells. New Phytol. **75:** 21–36.

LIZOTTE, M. P., AND J. C. PRISCU. 1994. Natural fluorescence and quantum yields in vertically stationary phytoplankton from perennially ice-covered lakes. Limnol. Oceanogr. **39:** 1399–1410.

MOBLEY, C. D. 1994. Light and water: Radiative transfer in natural water. Academic.

MOREL, A. 1988. Optical modeling of the upper ocean in relation to its biogenous matter content (case I waters). J. Geophys. Res. **93:** 10,749–10,768.

———, AND A. BRICAUD. 1981. Theoretical results concerning light absorption in a discrete medium, and application to specific absorption of phytoplankton. Deep-Sea Res. **28A:** 1375–1393.

———, AND L. PRIEUR. 1977. Analysis of variations in ocean color. Limnol. Oceanogr. **22:** 709–722.

Received: 8 July 1997
Accepted: 17 November 1997